J. Fluid Mech. (2015), *vol.* 769, *pp.* 729–739. © Cambridge University Press 2015
doi:10.1017/jfm.2015.156

Stabilization of a hypersonic boundary layer using a felt-metal porous coating

R. C. Tritarelli[1,2,†], S. K. Lele[2] and A. Fedorov[3]

[1]Institute of Fluid Dynamics, ETH Zürich, 8092 Zurich, Switzerland

[2]Department of Aeronautics and Astronautics, Stanford University, Stanford, CA 94305, USA

[3]Moscow Institute of Physics and Technology, Zhukovski, 140180, Russia

(Received 10 September 2014; revised 4 November 2014; accepted 19 December 2014; first published online 25 March 2015)

An error in the complex representation of the porous-coating model used in the study by Fedorov *et al.* (*J. Fluid Mech.*, vol. 479, 2003, pp. 99–124), investigating the stabilization effect of ultrasonically absorptive coatings on hypersonic boundary layers, is pointed out and corrected. This error has been acknowledged by Fedorov *et al.* (*J. Fluid Mech.*, vol. 769, 2015, pp. 725–728). The corrected version of the erroneous linear stability results of the original work is presented and previously made conclusions are reassessed. The novel numerical results indicate that second-mode instabilities are shifted to lower frequencies on felt-metal porous coatings, similar to the behaviour observed on porous coatings with regular microstructure.

Key words: boundary layer control, boundary layer stability, high-speed flow

1. Introduction and problem formulation

Several recent studies have shown experimentally (Rasheed *et al.* 2002), theoretically (Fedorov *et al.* 2001) and numerically (De Tullio & Sandham 2010) that porous coatings with a regular microstructure can stabilize second-mode disturbances in hypersonic boundary layers. Hence, these coatings may constitute an attractive passive laminar flow control technique for hypersonic boundary layers (Fedorov 2011).

Fedorov *et al.* (2003) investigated the stabilization properties of fibrous absorbent materials and presented for the first time a quantitative comparison between experimental and theoretical results regarding the effect of ultrasonically absorptive coatings (UACs) used for hypersonic laminar flow control. Fedorov *et al.* (2003) measured spectra of natural and artificially excited disturbances in a hypersonic boundary layer on a 7° half-angle sharp cone, which were used to compute experimental amplification curves and which were compared with results from linear stability theory (LST).

As will be shown in § 2, the numerical results for the porous-wall case in Fedorov *et al.* (2003) were erroneous due to incorrect boundary conditions. The corrected LST results are presented in § 3, where we discuss the stability properties of a hypersonic boundary layer on a solid and on a porous wall around a sharp cone with zero angle of attack. The mean-flow parameters are given in table 1, where M_e, T_e^* and Re_{1e}^* are the Mach number, temperature and unit Reynolds number at the boundary-layer edge respectively. Here, Re_{1e}^* is defined as $Re_{1e}^* := \sqrt{U_e^*/\nu_e^*}$, where U_e^*

† Email address for correspondence: tritarelli@ifd.mavt.ethz.ch

	M_e	T_e^* (K)	T_w	Re_{1e}^* (m^{-1})	γ	Pr	$\mathscr{R}^*$ (J kg^{-1} K^{-1})
Figures 1–3	5.3	59.3	5.5	15.5×10^6	1.4	0.708	287.1
Figure 4	5.3	59.3	2.0	10^7	1.4	0.708	287.1

TABLE 1. Mean-flow parameters for the studied hypersonic boundary layers.

and ν_e^* are the velocity and kinematic viscosity at the boundary-layer edge respectively. Additionally, table 1 gives the chosen numerical values for the heat capacity ratio γ, the Prandtl number Pr, the gas constant $\mathscr{R}^*$ and the non-dimensional wall temperature $T_w := T_w^*/T_e^*$. In table 1 as well as hereafter, $(\cdot)^*$, $(\cdot)_e$ and $(\cdot)_w$ represent dimensional quantities, variables at the boundary-layer edge and variables at the wall respectively.

In our analysis we will use the same problem formulation and numerical framework for the LST computations as discussed by Fedorov *et al.* (2003) with the exception of the corrected boundary conditions presented in § 2. We denote the non-dimensional mean-flow variables, i.e. pressure, temperature, density, streamwise and wall-normal velocity, as $P := P^*/(\rho_e^* U_e^{*2})$, $T := T^*/T_e^*$, $\rho := \rho^*/\rho_e^*$, $U := U^*/U_e^*$ and $V := V^*/U_e^*$ respectively. The coordinate system (x^*, y^*, z^*), used in the computations and representing the streamwise, wall-normal and spanwise direction, is non-dimensionalized with the boundary-layer length scale $l^* := \sqrt{\nu_e^* x^*/U_e^*}$, where x^* is the distance measured from the tip of the cone along the cone surface. The reference time is given by l^*/U_e^* and consequentially the non-dimensional time is $t := t^* U_e^*/l^*$ and the non-dimensional circular frequency can be defined as $\omega := \omega^* l^*/U_e^* = 2\pi f^* l^*/U_e^*$, where f^* is the dimensional frequency. As the numerical framework is the same as in Fedorov *et al.* (2003, 2015), the boundary-layer equations as well as the parallel and non-parallel linear stability equations used for the computations are given in Fedorov *et al.* (2003, 2015) and are not repeated in this paper. In conclusion, this implies that the normal-mode ansatz of equation (4.9) of Fedorov *et al.* (2003), where u, v, w, p and θ denote the disturbance amplitudes of the velocity components, of the pressure and of the temperature respectively, is used in this study. The computations in the remainder of the analysis are all performed in the framework of spatial linear stability analysis, hence we have $\omega \in \mathbb{R}$ for the circular frequency, $\beta := \beta^* l^* \in \mathbb{R}$ for the transverse wavenumber and $\alpha := \alpha^* l^* \in \mathbb{C}$ for the eigenvalue of the LST problem. The streamwise wavenumber can, hence, immediately be defined as $\alpha_r = \mathrm{Re}(\alpha)$.

2. Corrected porous-wall boundary condition

In the spatial linear stability calculations performed by Fedorov *et al.* (2003) the acoustic properties of a thin coating, made of a fibrous absorbent material (felt-metal), were described by the semi-empirical model of Allard & Champoux (1992) in conjunction with laboratory measurements of the felt-metal characteristics. Unfortunately, the equations describing the complex dynamic density $\widetilde{\rho} := \rho^*(\omega^*)/\rho_w^*$, the complex dynamic compressibility $\widetilde{C} := \gamma P_w^*/K^*(\omega^*)$, where $K^*(\omega^*)$ is the complex dynamic bulk modulus, and the propagation constant $\Lambda := \Lambda^* \cdot l^*$ were erroneous. The equations describing $\widetilde{\rho}$ and $\widetilde{C}$, i.e. equations (4.34)–(4.36) of the study by Fedorov *et al.* (2003), were chosen identical to those of the work by Allard & Champoux (1992) (equations (13) and (30) in conjunction with (46)), thereby neglecting the fact that the time dependences in the two studies are opposite. In the original work by

Allard & Champoux (1992) the harmonic time dependence was of the form $\exp(\mathrm{i}\omega t)$; however, Fedorov *et al.* (2003) used a time dependence of the form $\exp(-\mathrm{i}\omega t)$ in the normal-mode ansatz in equation (4.9). This change in time dependence requires a change in the characteristic impedance from $Z_0 := Z_0^*/(\rho_e^* U_e^*)$ to $Z_0^\dagger$, where $\dagger$ represents the complex conjugate. Similarly, it can be shown that the complex dynamic density $\widetilde{\rho}$, the complex dynamic compressibility $\widetilde{C}$, as well as the propagation constant Λ and the wall admittance A_y, are related via complex conjugation in both representations (Allard & Atalla 2009). This is a direct consequence of the fact that a real-valued pressure disturbance should yield a real-valued velocity disturbance, cf. Landau, Lifshitz & Pitaevskii (1984) and Johnson, Koplik & Dashen (1987).

Equations (4.34)–(4.36) in Fedorov *et al.* (2003) should consequently be replaced by

$$\widetilde{\rho} = a_\infty \left[1 + \frac{g(\lambda_1)}{\lambda_1}\right], \quad \widetilde{C} = \gamma - \frac{\gamma - 1}{1 + g(\lambda_2)/\lambda_2}, \tag{2.1a,b}$$

$$g(\lambda) = \sqrt{1 + \frac{4 a_\infty \mu_w^* \lambda}{\sigma^* \phi\, r_p^{*2}}}, \tag{2.2}$$

$$\lambda_1 = -\mathrm{i} a_\infty \rho_w^* \omega^* / (\phi \sigma^*), \quad \lambda_2 = 4 Pr \lambda_1, \tag{2.3a,b}$$

where a_∞, ϕ, σ^*, r_p^* and μ_w^* represent the tortuosity of the porous medium, the porosity, the flow resistivity, the characteristic viscous length scale inside the porous coating and the dynamic viscosity at the wall respectively. It should be noted that the tortuosity represents the high-frequency asymptotic limit of the dynamic density, i.e. $a_\infty = \lim_{\omega^* \to \infty} \widetilde{\rho}(\omega^*)$. The definition of the flow resistivity can be found in equation (4.37) of Fedorov *et al.* (2003), where furthermore the viscous length scale r_p^* was correctly defined in equation (4.40) as

$$r_p^* = \frac{\pi d^*}{2(1-\phi)(2-\phi)}, \tag{2.4}$$

with d^* referring to the diameter of the stainless steel fibres of the felt-metal coating. It should be highlighted that equation (4.39) for r_p^* of Fedorov *et al.* (2003) was erroneous, see Fedorov *et al.* (2015). The definition of the porosity ϕ is given in (A 7).

Equations (2.1)–(2.3) correspond to the porous-media model derived by Allard & Champoux (1992), which can be considered to be a special case (applicable to fibrous absorbent materials only) of the model by Champoux & Allard (1991). The model by Allard & Champoux (1992) was derived for a material with non-touching fibres. Fedorov *et al.* (2003) applied this model to a UAC with touching fibres and therefore decided to evaluate r_p^* differently from Allard & Champoux (1992). In Fedorov *et al.* (2003) the pore size r_p^* was treated as a hydraulic radius, which was defined as the radius of the equivalent pore. It was derived based on a statistical analysis (see appendix A).

Compared with the original work, changing the sign of λ_1 in equation (4.36) of Fedorov *et al.* (2003) results in (2.3); this makes the model compatible with the time dependence $\exp(-\mathrm{i}\omega t)$ and thereby yields the correct values for $\widetilde{\rho}$ and $\widetilde{C}$.

The correct boundary conditions for the linear stability computations, replacing equations (4.31)–(4.33) of Fedorov *et al.* (2003), can now be written in non-dimensional form as

$$y = 0: \quad u = w = \theta = 0, \quad v = A_y p, \tag{2.5a,b}$$

a_∞	σ^* (kg m^{-3} s^{-1})	ϕ	d^* (μm)	h^* (mm)
1	1.66×10^5	0.75	30	0.75

TABLE 2. Numerical parameters describing the felt-metal coating.

$$A_y = -\frac{\phi}{Z_0}\tanh(\Lambda h), \tag{2.6}$$

$$Z_0 = \frac{\sqrt{\widetilde{\rho}/\widetilde{C}}}{M_e\sqrt{T_w}}, \quad \Lambda = -\frac{\mathrm{i}\omega M_e}{\sqrt{T_w}}\sqrt{\widetilde{\rho}\,\widetilde{C}}, \tag{2.7a,b}$$

where $h := h^*/l^*$ is the non-dimensional porous-layer thickness and where (2.7) is obtained after the non-dimensionalization of the characteristic impedance Z_0^* and the propagation constant Λ^*, given by $Z_0^* = \sqrt{\rho^*(\omega^*)K^*(\omega^*)}$ and $\Lambda^* = -\mathrm{i}\omega^*\sqrt{\rho^*(\omega^*)/K^*(\omega^*)}$. In the definition of the admittance A_y in (2.6), the minus sign is required because an excess pressure induces a flow into the wall (in the $-y$ direction). In Fedorov *et al.* (2003) the minus sign due to the direction of propagation was incorporated into the definition of Z_0; however, in the present work $\mathrm{Re}(Z_0) > 0$ is preferred. Additionally, it should be highlighted that the sign of the propagation constant Λ was changed in comparison to Fedorov *et al.* (2003), in order to make the boundary condition compatible with the normal-mode ansatz.

The numerical parameters needed for the evaluation of the boundary conditions and the porous-coating model are given in table 2, with the exception of the dynamic viscosity μ_w^*, which is given by Sutherland's law as

$$\mu_w^* = 1.458 \times 10^{-6}\,\frac{T_w^{*3/2}}{T_w^* + C^*}, \tag{2.8}$$

with $C^* = 110.4$ K in accordance with the non-dimensional form of the Sutherland law, which was used in the boundary-layer and stability equations, i.e.

$$\mu := \mu^*/\mu_e^* = \frac{1+S}{T+S}\,T^{3/2} \tag{2.9}$$

with $S = 110.4/T_e^*$.

It should be mentioned that, although equations (4.34)–(4.36) in Fedorov *et al.* (2003) provided an incorrect representation of the porous coating, the identification of the felt-metal flow resistivity σ^* via the method of acoustic standing waves provided the correct results. Despite the fact that the predicted imaginary parts of Z_0, of A_y and of the reflection coefficient for plane acoustic waves of normal incidence R_{ref}, which can be expressed as

$$R_{ref} := \frac{M_e\sqrt{T_w} + A_y}{M_e\sqrt{T_w} - A_y}, \tag{2.10}$$

have the wrong sign in Fedorov *et al.* (2003), the results in figure 12 remain correct as the normal-incidence energy absorption coefficient $K_a := 1 - |R_{ref}|^2 = 1 - |R_{ref}^\dagger|^2$ is taken as the basis for the identification of σ^*, which therefore is not affected by the erroneous time dependence. The experimentally obtained value of σ^* in Fedorov *et al.* (2003) can consequently be used in the present work in order to complete the semi-empirical model presented in equations (2.1)–(2.4).

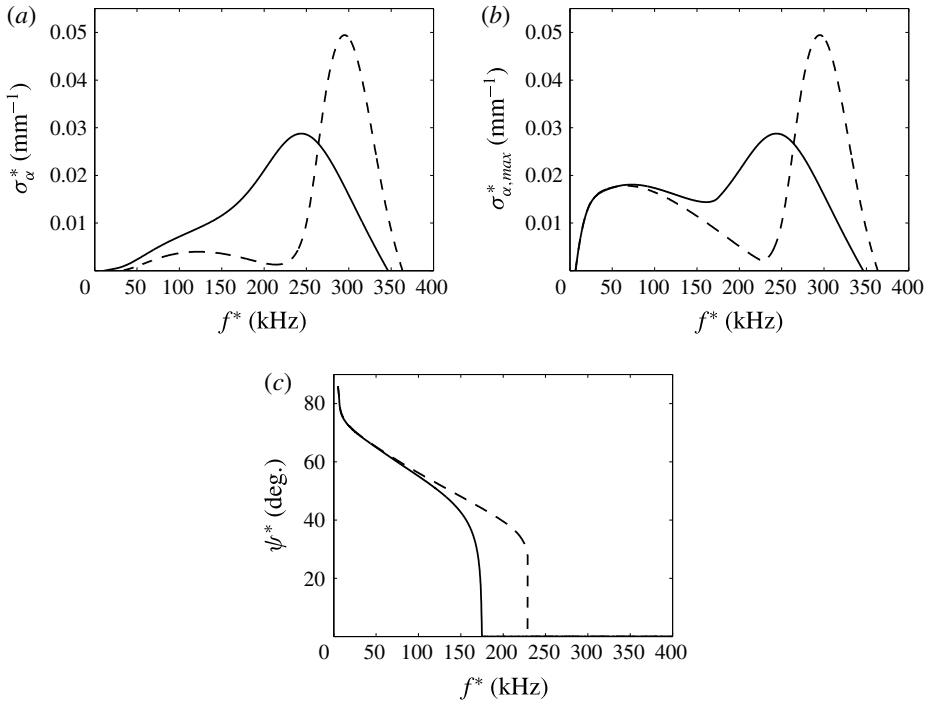

FIGURE 1. (*a*) Growth rate of two-dimensional disturbances versus frequency at $x^* = 200.1$ mm ($R = 1761.2$); locally parallel approximation. (*b*) Maximum growth rate of three-dimensional disturbances versus frequency at $x^* = 200.1$ mm ($R = 1761.2$); locally parallel approximation. (*c*) The wave angle $\psi^* = \arctan(\beta/\alpha_r)$ of the most unstable three-dimensional waves versus frequency at $x^* = 200.1$ mm ($R = 1761.2$); locally parallel approximation. Dashed lines: solid wall; solid lines: porous wall with the corrected boundary condition. Correction of figure 13 of Fedorov *et al.* (2003).

3. Stability calculations and comparison with experiment

3.1. *Linear stability calculations*

In this section the corrected version of the erroneous linear stability results of Fedorov *et al.* (2003) is presented. Figures 1, 2 and 4 present the corrected results of figures 13, 14 and 17 of Fedorov *et al.* (2003) respectively. Figure 1(*a*) depicts the growth rate of two-dimensional disturbances $\sigma^*_\alpha(x^*, f^*, \beta^* = 0)$ in a boundary layer corresponding to the mean-flow parameters given in table 1 at a position x^* equivalent to a Reynolds number $R := U^*_e l^*/\nu^*_e = \sqrt{U^*_e x^*/\nu^*_e}$ of $R = 1761.2$. The growth rate $\sigma^*_\alpha(x^*, f^*, \beta^*)$ is defined as $\sigma^*_\alpha := -\mathrm{Im}(\alpha^*)$ for the case of locally parallel LST. For the definition of σ^*_α applicable in the case of the non-parallel LST, we refer to Fedorov *et al.* (2003). Additionally, figure 1 presents the maximum growth rate of three-dimensional disturbances, i.e. $\sigma^*_{\alpha,max} := \max_{\beta^*}[\sigma^*_\alpha(x^*, f^*, \beta^*)]$, and the corresponding wave angle ψ^*. Figure 2 presents similar results for a different position in the boundary layer. Figures 1 and 2 correspond to the experimental conditions of Fedorov *et al.* (2003). Whereas these conditions represent a nearly adiabatic wall temperature, figure 4 represents a scenario with a cooled wall.

The stabilization of the second-mode disturbances due to the porous coating is also observed with the corrected boundary conditions in figures 1, 2 and 4, similarly to

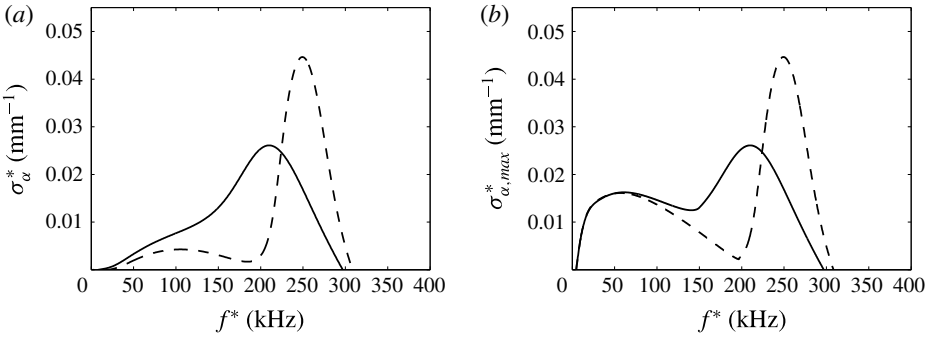

FIGURE 2. (*a*) Growth rate of two-dimensional disturbances versus frequency at $x^* = 283.2$ mm ($R = 2095$); locally parallel approximation. (*b*) Maximum growth rate of three-dimensional disturbances versus frequency at $x^* = 283.2$ mm ($R = 2095$); locally parallel approximation. Dashed lines: solid wall; solid lines: porous wall with the corrected boundary condition. Correction of figure 14 of Fedorov *et al.* (2003).

the original results. Furthermore, it can be seen that the porous medium shifts the maximum growth rate associated with second-mode disturbances to lower frequencies. This observation is in accordance with earlier studies of the stabilization effect of porous coatings with regular microstructure, i.e. circular cylindrical holes, performed by Fedorov *et al.* (2001), whose results remain unaffected by the present analysis. The shift of the second-mode instability to lower frequencies therefore seems to be independent of the particular porous coating under investigation. This conclusion is in disagreement with the originally presented results, which indicated that the felt-metal coating shifts the second-mode instability to higher frequencies. This difference can be observed best when figure 17 of Fedorov *et al.* (2003) is compared with the present figure 4.

As a direct consequence of the observed frequency shift, the changeover from the oblique first-mode instability to the two-dimensional second-mode instability takes place at lower frequencies, as can be observed by comparing the results of figure 13(*c*) of Fedorov *et al.* (2003) with figure 1(*c*). Apart from the shift of the frequency, a considerably increased value of the maximum second-mode growth rate is observed with the corrected boundary condition, indicating a strong dependence of the stabilization on the phase of the wall admittance and thereby indicating that the norm of the reflection coefficient of the wall is not a good criterion for the design of porous coatings.

The corrected linear stability results help to explain the presence of the low-frequency lobe in the disturbance spectrum for natural disturbances measured on the porous surface (see figure 4(*b*) of Fedorov *et al.* 2003). This lobe in the frequency band from 100 to 200 kHz was originally attributed to the destabilization of the first mode. As a consequence of the aforementioned corrected results, it can be concluded that the presence of this lobe is associated with two independent trends: along with the increase of the first-mode growth rate there is a shift of the second-mode instability to lower frequencies, as can be seen in figure 2(*a*). The importance of this shift is emphasized if the ratio $A_f(\mathrm{S5})/A_f(\mathrm{S1})$ is analysed. This corresponds to the ratio of the disturbance amplitude at location S5 ($x^* = 289.4$ mm) and location S1 ($x^* = 189.1$ mm), near the leading edge of the porous surface ($x^* = 187$ mm), where the experimental mass-flow disturbance amplitude $A_f(x^*, \Theta^*, f^*)$ for natural

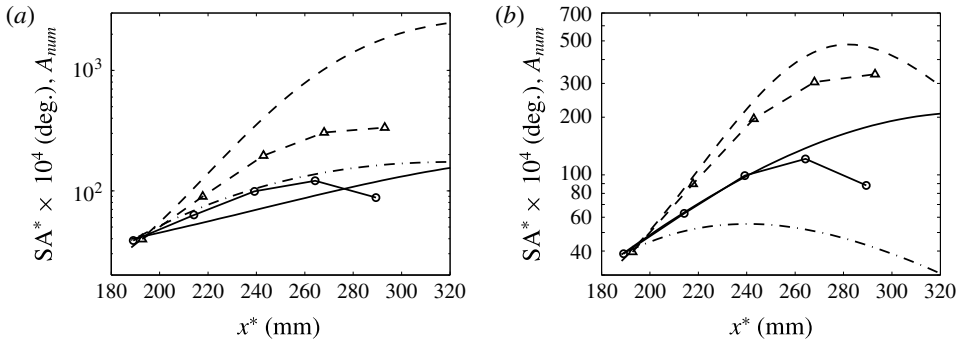

FIGURE 3. Amplification of the two-dimensional component of the artificially excited wavepacket of frequency $f^* = 280$ kHz, i.e. $\mathrm{SA}^*(x^*, \beta^*_{exp} = 0)$, versus the theoretical amplification curve A_{num}; (*a*) locally parallel theory versus experiment, (*b*) non-parallel theory versus experiment. Theoretical result for the solid-wall case (dashed lines), theoretical result for the porous-wall case with the corrected boundary condition (dot-dashed lines), theoretical result for the porous-wall case as presented in Fedorov *et al.* (2003) (solid lines), experiment on the solid wall (dashed lines with △ symbol), experiment on the porous wall (solid lines with ○ symbol). Correction of figures 15 and 16 of Fedorov *et al.* (2003).

disturbances and its corresponding phase Φ^*_f are computed via the discrete Fourier transform, i.e.

$$A_f(x^*, \Theta^*, f^*)\exp(\mathrm{i}\Phi^*_f(x^*, \Theta^*, f^*)) := \frac{2}{N}\sum_{j=1}^{N} \dot{m}'_{max}(x^*, \Theta^*, t^*_j)\exp(-2\pi\mathrm{i}f^* t^*_j). \quad (3.1)$$

Here, N denotes the sample count, Θ^* is the circumferential angle on the cone and $\dot{m}'_{max}$ is the maximum of the non-dimensional mass-flow disturbance $\dot{m}'$, which is defined as $\dot{m}' := \rho' U + \rho U'$, where ρ' and U' are the experimentally measured density disturbance and velocity disturbance respectively. In the experiments the maximum of the mass-flow disturbance is computed over the coordinate normal to the axis of the cone. Analogously to A_f and Φ^*_f for natural disturbances, the amplitude $A(x^*, \Theta^*)$ and the phase $\Phi^*(x^*, \Theta^*)$ can be defined for artificially excited disturbances of a given frequency f^*. The disturbance amplitudes plotted in figure 4 of Fedorov *et al.* (2003) were measured at a circumferential angle of $\Theta = 0°$.

The ratio $A_f(\mathrm{S5})/A_f(\mathrm{S1})$, which corresponds to the growth of the instability on the porous surface, has a peak between 150 and 250 kHz and can most likely be associated with a second mode, see figure 2(*a*). However, the presence of the lobe cannot be attributed definitely to one or the other mode, as the frequency ranges of both modes are overlapping for the porous-wall case, which is also apparent from the computational results, e.g. figure 2(*a*). This conclusion is drastically different from the conclusion made by Fedorov *et al.* (2003), who believed that the low-frequency lobe is due entirely to first-mode instabilities.

3.2. *Comparison of numerical and experimental amplification curves*

Figures 3(*a*) and (*b*) present the correction of figures 15 and 16 of the original paper and present a comparison between theoretical and experimental amplification

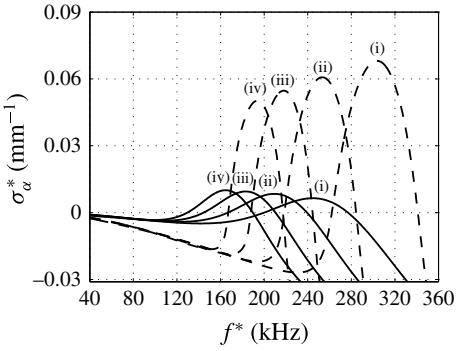

FIGURE 4. Growth rate of two-dimensional disturbances as a function of frequency f^* at various x^*, $T_w^* = 2\ T_e^*$, $Re_{1e}^* = 10^7$ m^{-1}; locally parallel approximation; (i) $x^* = 206.35$ mm, (ii) $x^* = 298.72$ mm, (iii) $x^* = 406.05$ mm, (iv) $x^* = 515.79$ mm. Dashed lines: solid wall; solid lines: porous wall with the corrected boundary condition. Correction of figure 17 of Fedorov *et al.* (2003).

curves. The experimental amplification curve represents the amplification of the two-dimensional component of the artificially excited wavepacket, denoted SA* $(x^*, \beta_{exp}^* = 0)$, where β_{exp}^* is the azimuthal wavenumber. The azimuthal wavenumber β_{exp}^* used in the experiments ($[\beta_{exp}^*] = $ rad deg^{-1}) should be discerned from the transverse wavenumber β^* used in the linear stability calculations ($[\beta^*] = $ rad m^{-1}). The amplitude SA* of the azimuthal wavenumber β_{exp}^* component and its corresponding phase SF* can be determined via

$$\mathrm{SA}^*(x^*, \beta_{exp}^*)\exp(\mathrm{iSF}^*(x^*, \beta_{exp}^*)) := \int_{-\Theta_0^*}^{\Theta_0^*} A(x^*, \Theta^*)\exp(\mathrm{i}(\Phi^*(x^*, \Theta^*) - \beta_{exp}^*\Theta^*))\mathrm{d}\Theta^*, \tag{3.2}$$

where the limit of integration Θ_0^* was chosen in order to cover the entire wavepacket in the experiments, and where the amplitude $A(x^*, \Theta^*)$ was calculated for artificially exited disturbances with a frequency of $f^* = 280$ kHz. The experimentally obtained amplification curve is compared with the numerical amplification curve $A_{num}(x^*)$, defined as

$$A_{num}(x^*) := A_{num,0}\exp\left(\int_{x_1^*(S_1)}^{x^*} \sigma_\alpha^*(\widetilde{x}^*, f_0^*, 0)\mathrm{d}\widetilde{x}^*\right), \tag{3.3}$$

where $A_{num,0}$ is the amplitude at position S1, which is adjusted to match the experimental results. The local growth rate for two-dimensional disturbances, is determined by either the locally parallel LST or the non-parallel LST. For the results presented in figure 3, the local growth rate was computed for a fixed frequency of $f^* = f_0^* = 280$ kHz and for the mean-flow parameters given in table 1.

Comparing the experimental and numerical results in figure 3, we can see that with the corrected boundary condition, the theoretical results on the porous wall based on the parallel flow assumption are in better agreement with the experimental measurements than the originally published results (see figure 3(*a*)). In opposition to this improved agreement for the locally parallel theory, the results based on the weakly non-parallel theory show a considerable discrepancy compared with the experimental data for the porous-wall case, for which in Fedorov *et al.* (2003) a

nearly perfect agreement was erroneously observed (see figure 3(*b*)). Compared with the locally parallel theory, the non-parallel theory predicts a smaller amplification for the solid wall and for the porous wall. This observation is in opposition to the results of Fedorov *et al.* (2003), where the non-parallel theory predicted an increased amplification for the porous-wall case. The fact that for the porous-wall case the presumably more accurate non-parallel theory shows less satisfactory agreement with the experimental results needs to be analysed in the future. At this point, one needs to be reminded that the growth rate of the non-parallel theory is dependent on the distortion of the eigenfunction and therefore is affected by the choice of the disturbance norm and the location of its evaluation. In the present work, the disturbance measure was given by the mass-flow disturbance, which was evaluated at the wall-normal location of the maximum mass-flow disturbance. Additionally, it is reasonable to mention that the distributed roughness of the felt-metal surface could lead to additional growth of the boundary-layer disturbances. In the experiments, acoustic noise present in the hypersonic wind tunnel could interact with this roughness, which could lead to a downstream increase in the disturbance amplitude. The linear stability theory does not account for this effect, which could be present in the experiment. Therefore, it is natural to assume that the stability theory can overpredict the UAC performance. This is consistent with the results shown in figure 3(*b*).

4. Conclusion

An inconsistency between the normal-mode ansatz and the complex representation of the felt-metal-coating model in the study of Fedorov *et al.* (2003) has been pointed out and corrected. Furthermore, the resulting corrected linear stability calculations have been presented.

The present corrected results, which indicate a shift of second-mode disturbances to lower frequencies due to felt-metal coatings, help to explain the experimentally obtained spectra of natural disturbances on the porous wall, as shown in figure 4(*b*) of Fedorov *et al.* (2003). The large amplitude of the disturbances in the low-frequency range from 100 to 200 kHz can be attributed to a destabilization of first-mode disturbances and a shift of second-mode disturbances to lower frequencies on the felt-metal coating. This shift to lower frequencies of the second mode is in accordance with results for porous coatings with a regular microstructure and therefore seems to be a feature independent of the type of the porous coating under investigation.

Additionally, it was observed that the locally parallel linear stability analysis on the porous wall using the corrected boundary conditions shows an improved agreement with the experimental results.

The major results of the linear stability analysis by Fedorov *et al.* (2003) remain unaltered, i.e. the strong stabilization of second-mode disturbances and the minor destabilization of first-mode disturbances are also observed with the corrected boundary conditions. The conclusion that ultrasonically absorptive coatings may be an attractive laminar flow control technique for hypersonic boundary layers remains valid.

Acknowledgements

R.C.T. acknowledges K. Franko from Stanford University for several fruitful discussions, as well as the Excellence Scholarship and Opportunity Programme (ESOP) and Professor L. Kleiser of ETH Zürich for financial support. This work was supported partially (A.F.) by the Russian Scientific Foundation (project no. 14-19-00821).

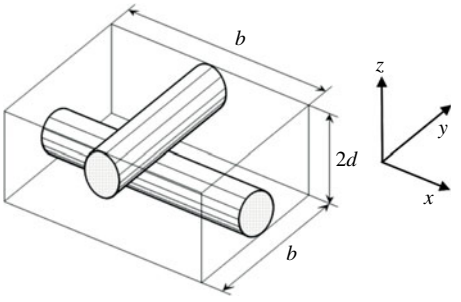

FIGURE 5. An elementary cell of the felt-metal microstructure: a parallelepiped of dimension $b \times b \times 2d$ including two adjoining sections of fibres with diameter d and mutually orthogonal axis (modified figure 11 of Fedorov *et al.* (2003), reprinted with permission of the authors).

Appendix A. Statistical derivation of the viscous length scale r_p^*

In Fedorov *et al.* (2003) the viscous length scale r_p^* was not evaluated based on equation (4.38), as was done in Allard & Champoux (1992). Rather, the expression for r_p^* was derived by using a statistical analysis of the elementary cell shown in figure 5. Unfortunately, the details of the derivations were omitted in the original publication and are given below.

Making use of an analogy with the kinetic theory of rarefied gases, we consider a one-dimensional uniform stream of molecules within the porous material. The molecules are colliding with the solid frame of the porous material. It is assumed that the collision frequency per unit volume, $\mathscr{Z}_{FM}^*$, for molecules moving parallel to the felt-metal (FM) surface (in the (x, y)-plane) is proportional to the projected area of fibres, i.e.

$$\mathscr{Z}_{FM}^* = \mathscr{B}^*(n_M^*, \bar{c}^*) \cdot n_S^* \cdot (S_{xz}^* + S_{yz}^*), \tag{A 1}$$

where n_M^* is the number of molecules per unit volume, n_S^* is the cell density (average number of elementary cells per unit volume), $\bar{c}^*$ is the average molecular speed, and S_{xz}^* and S_{yz}^* are the areas of the fibres projected to the (x, z)-plane and (y, z)-plane respectively. The parameter $\mathscr{B}^*$ characterizes the number of molecules colliding with a unit surface area per unit time. For a rarefied gas, i.e. for Knudsen numbers $Kn \gg 1$, it can be expressed explicitly as $\mathscr{B}^* = n_M^* \bar{c}^*/4$. For small Knudsen numbers, $\mathscr{B}^*(n_M^*, \bar{c}^*)$ can differ from the expression for a rarefied gas. However, this does not affect the final result. Based on figure 5, the projected areas can be computed as

$$S_{xz}^* = S_{yz}^* = d^* b^* \left(1 + \frac{\pi d^*}{4 b^*}\right) \tag{A 2}$$

and the cell density can be evaluated as

$$n_S^* = \frac{1}{2 d^* b^{*2}}, \tag{A 3}$$

where b^* is the cell size of an elementary cell of the felt-metal microstructure. Substitution of n_S^*, S_{xz}^* and S_{yz}^* in (A 1) yields

$$\mathscr{Z}_{FM}^* = \mathscr{B}^* \frac{\left(1 + \dfrac{\pi d^*}{4 b^*}\right)}{b^*} \tag{A 4}$$

for the collision frequency inside the felt-metal.

The same calculation can be performed for a long cylindrical pore of radius r^* and height $\mathscr{H}^*$, with the axis of the cylindrical pore directed along the z-axis. The collision frequency for this configuration reads

$$\mathscr{Z}^*_{Cyl} = \mathscr{B}^* \frac{2\pi r^* \mathscr{H}^*}{\pi r^{*2} \mathscr{H}^*} = \mathscr{B}^* \frac{2}{r^*}. \tag{A 5}$$

The collision frequencies $\mathscr{Z}^*_{Cyl}$ and $\mathscr{Z}^*_{FM}$ can be equated in order to obtain the radius of the equivalent pore,

$$r^*_p = \frac{2b^*}{1 + \dfrac{\pi d^*}{4b^*}}. \tag{A 6}$$

Equation (A 6) can be combined with the expression for the porosity of the felt-metal, i.e.

$$\phi = 1 - \frac{\pi d^*}{4b^*}, \tag{A 7}$$

in order to obtain

$$r^*_p = \frac{\pi d^*}{2(1-\phi)(2-\phi)}. \tag{A 8}$$

Equation (A 8) coincides with equation (4.40) of the original paper and was used together with (A 7) in all the numerical computations of the present as well as the original paper. The erroneous equation (4.39) of the original paper was unfortunately used in the analysis of Wang & Zhong (2012).

REFERENCES

ALLARD, J. F. & ATALLA, N. 2009 *Propagation of Sound in Porous Media: Modelling Sound Absorbing Materials*, 2nd edn. John Wiley & Sons.

ALLARD, J.-F. & CHAMPOUX, Y. 1992 New empirical equations for sound propagation in rigid frame fibrous materials. *J. Acoust. Soc. Am.* **91** (6), 3346–3353.

CHAMPOUX, Y. & ALLARD, J.-F. 1991 Dynamic tortuosity and bulk modulus in air-saturated porous media. *J. Appl. Phys.* **70** (4), 1975–1979.

DE TULLIO, N. & SANDHAM, N. D. 2010 Direct numerical simulation of breakdown to turbulence in a Mach 6 boundary layer over a porous surface. *Phys. Fluids* **22** (9), 094105.

FEDOROV, A. 2011 Transition and stability of high-speed boundary layers. *Annu. Rev. Fluid Mech.* **43**, 79–95.

FEDOROV, A., SHIPLYUK, A., MASLOV, A., BUROV, E. & MALMUTH, N. 2003 Stabilization of a hypersonic boundary layer using an ultrasonically absorptive coating. *J. Fluid Mech.* **479**, 99–124.

FEDOROV, A., SHIPLYUK, A., MASLOV, A., BUROV, E. & MALMUTH, N. 2015 Stabilization of a hypersonic boundary layer using an ultrasonically absorptive coating – CORRIGENDUM. *J. Fluid Mech.* **769**, 725–728.

FEDOROV, A. V., MALMUTH, N. D., RASHEED, A. & HORNUNG, H. G. 2001 Stabilization of hypersonic boundary layers by porous coatings. *AIAA J.* **39** (4), 605–610.

JOHNSON, D. L., KOPLIK, J. & DASHEN, R. 1987 Theory of dynamic permeability and tortuosity in fluid-saturated porous media. *J. Fluid Mech.* **176**, 379–402.

LANDAU, L. D., LIFSHITZ, E. M. & PITAEVSKII, L. P. 1984 *Electrodynamics of Continuous Media*, 2nd edn. Pergamon.

RASHEED, A., HORNUNG, H. G., FEDOROV, A. V. & MALMUTH, N. D. 2002 Experiments on passive hypervelocity boundary-layer control using an ultrasonically absorptive surface. *AIAA J.* **40** (3), 481–489.

WANG, X. & ZHONG, X. 2012 The stabilization of a hypersonic boundary layer using local sections of porous coating. *Phys. Fluids* **24** (3), 034105.